# Zeolites in a good shape: Catalyst forming by extrusion modifies their performances

Louwanda Lakiss, Jean-Pierre Gilson, Valentin Valtchev, Svetlana Mintova, Aurélie Vicente, Alexandre Vimont, Robert Bedard, Suheil Abdo, Jeffery Bricker

# Zeolites in a Good Shape: Catalyst Forming by Extrusion Modifies their Performances

Louwanda Lakiss, [a]Jean-Pierre Gilson, *[a] Valentin Valtchev, [a] Svetlana Mintova, [a] Aurélie Vicente, [a] Alexandre Vimont, [a] Robert Bedard, [b] Suheil Abdo, *[b] and Jeffery Bricker [b]

Chemical interactions occurring between zeolites and alumina binders during the critical steps of catalyst forming are the focus of this study. Three widely used and commercially significant variants of FAU zeolite, covering a wide range of Si/Al ratios, micro- and meso-porosity and acidic properties (Y [LZY-64, Si/Al = 2.3] and USY [CBV 720 and CBV 760 with Si/Al = 16 and Si/Al = 28, respectively]) were shaped by extrusion with pseudoboehmite to produce bound extrudates. These extrudates were characterized by conventional techniques (XRD, $^{27}$Al NMR and IR spectroscopy, $N_2$ physisorption...) and compared to their parent powders activated under the same conditions. The catalytic performances of the zeolite powders, their derived alumina extrudates and physical zeolite/ γ-$Al_2O_3$ mixtures were also evaluated employing two different reactions: *i*) n-octane hydroisomerization, to probe all catalytic sites and *ii*) 1,3,5 tri-isopropyl benzene dealkylation to probe only the external/mesoporous surfaces. The bound zeolites systematically displayed catalytic performance superior to their parent powders or physical mixtures, especially in the dealkylation of 1,3,5 tri-isopropyl benzene. Infrared spectroscopy measurements of the number, nature and strength of the acid sites were consistent with these catalytic results demonstrating that new catalytic sites are created and located on the external or mesoporous surface of the zeolites, *i.e.* at the zeolite-binder interface. The work reported here clearly illustrates that binding and subsequent thermal treatment of zeolite powders to produce commercially representative forms can significantly alter the quality and quantity of active sites creating active centers not usually present in pure powders which are typically studied and reported in much of the open literature. Such a study is also a blueprint for other catalytic phases, other forming processes (spray-drying, oil-dropping, pelletizing…) and could also be applied to the shaping of adsorbents.

**Keywords:** Zeolite, Binder, Faujasite, Extrudates, Catalysis, Shaping

## Introduction

With few exceptions, most academic research on (zeolitic) catalysts is performed on pure powders even though they are always formed into various shapes using binders in commercial application.[1,2,3,4,5,6,7,8] In industry, catalyst forming, a critical step in the scaling-up of promising laboratory prototypes, is normally practiced using empirically acquired know-how generally kept as trade-secrets. The net result is a scarcity of robust scientific background in the open literature related to this academically exciting and industrially relevant topic.

Heterogeneous catalysts and adsorbents are shaped to optimize many, often conflicting, requirements such as mechanical and thermal resilience, hydrodynamics of reactants and products, accessibility to a maximum number of catalytic/adsorption sites and the need to transport a deactivated catalyst from a reactor to a regenerator.[9] The most common shapes, such as extrudates (~2 mm diameter), mini-spheres (~2 mm diameter) and micro-spheres (~70 µm diameter), are often imposed by the deactivation rates which, for example, are measured in months for fixed beds such as Hydrocracking, days for mini-spheres employed in Continuous Catalytic Reforming and seconds for micro-spheres utilized in Fluid Catalytic Cracking, Figure 1.[10,11,12] During the forming steps in commercial catalyst production, a zeolite is typically first mixed and kneaded with an inorganic binder precursor (*e.g.* pseudoboehmite) and other additives (peptizing agents, porogens, fillers…), formed through a die yielding so called green extrudates, dried and then calcined. During these operations, it is well known in industry but not yet fully appreciated in academia, that chemical interactions may take place between the binder and the active phase leading to performance properties that are much in need of fundamental understanding and quantification.[13,14]

The field was recently reviewed and it is apparent that a range of, at times, conflicting conclusions have been reached in some studies related to this phenomenon.[1,2] Verkleij *et al*. concluded that the nature of the binder employed in their study barely affects selectivity and deactivation rate in 1-hexene oligomerization.[15] Lee *et al.*

[a] Normandie Univ, ENSICAEN, UNICAEN, CNRS, Laboratoire Catalyse et Spectrochimie, 14000 Caen, France.
E-mail: jean-pierre.gilson@ensicaen.fr
[b] UOP LLC, 25 East Algonquin Road, Des Plaines, IL 60016, USA.
E-mail: suheil.abdo@honeywell.com
* Electronic supplementary information (ESI) available. Additional nitrogen sorption analyses and catalytic selectivity.

reported that, in the MTO (Methanol to Olefins) process, bound zeolites displayed better catalytic performances (activity, deactivation) than their parent powder.[16] Pérez-Ramírez *et al.* also reported that formed hierarchical ZSM-5 catalysts have a direct impact on their catalytic performances during the MTO reaction.[17] Their bound catalysts exhibited higher macroporosity and better mass transport properties while preserving their native intracrystalline mesoporosity.[18] Others also reported that catalytic activity could be reduced during forming due to the agglomeration of binder around the active phase.[19,20]

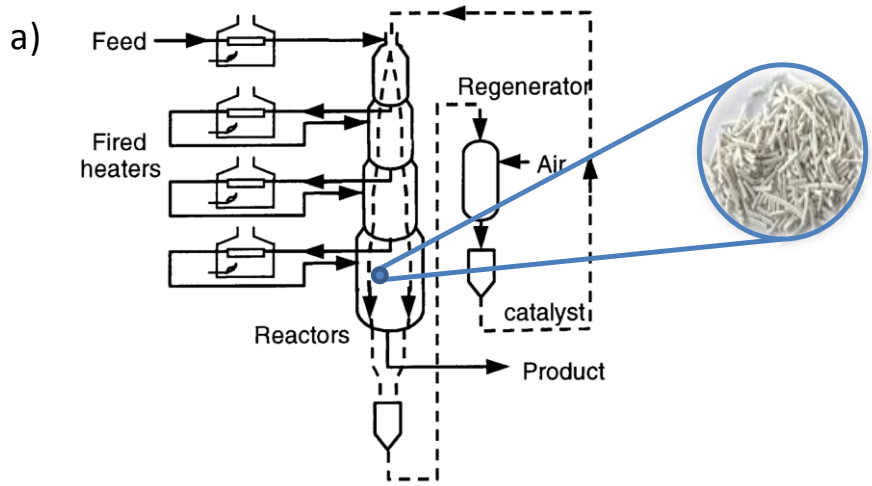


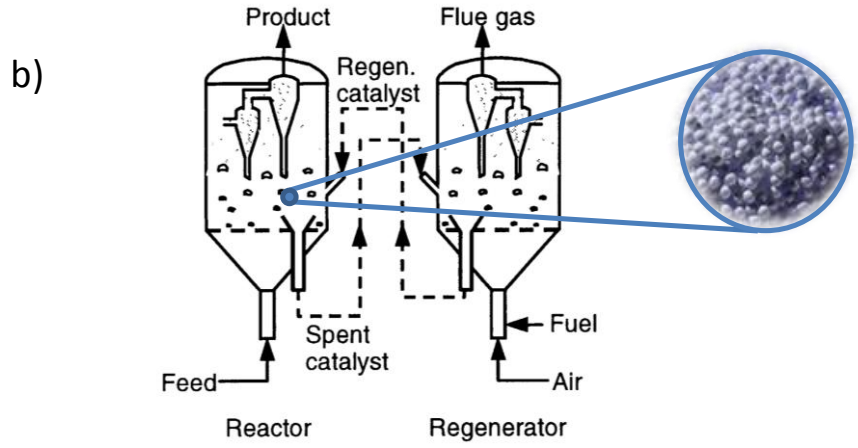


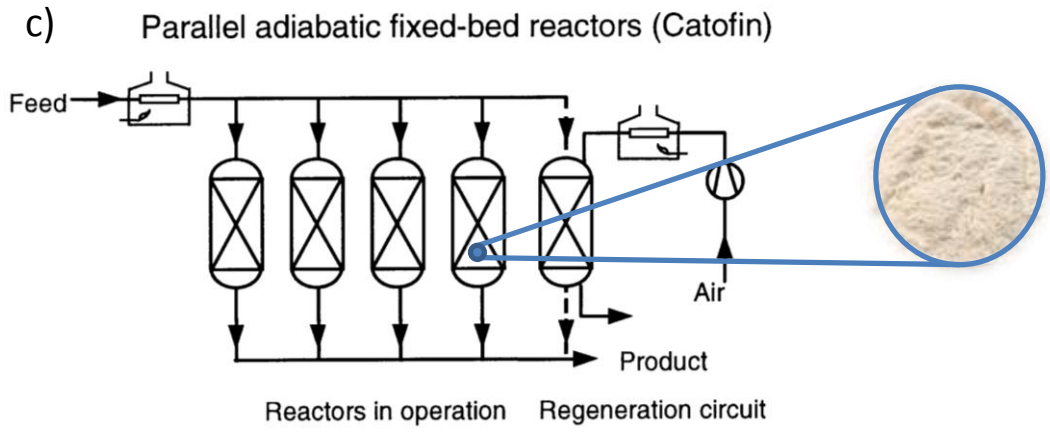

**Figure 1.** Commercially available technologies and associated catalyst shapes to manage deactivation *a*) Fixed beds with extrudates (catalyst lifetime: months), *b*) Moving beds with millimeter-sized spheres (catalyst lifetime: days), *c*) Fluidized beds with micron-sized spheres (catalyst lifetime: seconds) Adapted from ref. 11.

Earlier, Shihabi *et al*. discovered that ZSM-5/alumina extrudates displayed better catalytic performances than intimate physical mixtures of ZSM-5 and alumina in propylene oligomerization.[21] They also reported that an alumina binder can be a source of mobile species modifying the catalytic performances of zeolite extrudates in n-hexane cracking, propylene oligomerization, lube dewaxing and the transformation of methanol to hydrocarbon.[22] An interesting conclusion was communicated by Noronha *et al.* who demonstrated that mordenite embedded in matrices are better protected against thermal degradation than physical mixtures of the zeolite and its matrix.[23] Clearly, some of the evolution in zeolite performance upon binding and subsequent calcination is related to the mobility of aluminum species as shown by Valtchev *et al.* who studied the evolution of a binder during the different stages of pellets preparation.[24] Corma *et al*. and de la Puente *et al.* also reported the migration of aluminum species during the steaming of silica bound USY zeolites resulting in the formation of a new silica alumina phase.[25,26] Bifunctional MOR and MFI (Pt and Pd loaded) zeolites bound with bentonite displayed better branching selectivity in n-octane hydroisomerization than their unbound parents; the authors attributed this improvement to enhanced diffusion due to the additional meso- and macro-porosity provided by the binder.[27,17] Employing advanced nanoscale characterization techniques, the Weckhuysen group recently revisited zeolite-binder interactions during forming of FCC catalysts and concluded that intimate contact between a zeolite and its binder can have a profound impact on catalytic performances and that the nature of binder plays a key role in determining the outcome.[28,29,30] Much literature (reviews, book chapters, patents…) deals with shaping and binding catalysts in different forms such as pellets, monoliths, granules, or extrudates, but mostly from a materials science perspective.[31] However, an integrated study including *i)* deliberate control of the nature of the starting materials (zeolite and binder) and forming parameters *ii)* spectroscopic characterization of the powders and formed catalysts, *iii)* evaluation of catalytic performances is still needed. Thus, a more detailed scientific investigation of this topic is warranted to better understand the influence of the forming process with the hope that the knowledge generated leads to a better design of industrially relevant catalysts and adsorbents. This is even more relevant in the case of zeolite-based catalysts as the most favored binders ($Al_2O_3$, $SiO_2$, clays and $AlPO_4$) are generally chemically related leading to the expectation that chemical interactions are likely to take place during forming.[32,]**Erreur ! Signet non défini.** With this background in mind, we set out to investigate the impact of forming by extrusion on various forms of FAU zeolites (Si/Al ratios, texture) by comparing a zeolite Y and two ultra-stabilized Y zeolites (USY-1 and USY-2). The questions addressed are two-fold:
- when and where do the critical zeolite-binder interactions take place, if any?
- what is the nature and the catalytic consequences of these interactions?

Herein, characterization results of the parent zeolite powders, physical mixtures of zeolites and binders and their formed and bound derivatives using the appropriate characterization tools will be presented along with their catalytic performance in two test reactions selected to probe all catalytic sites (n-$C_8$ hydroisomerization) or those specifically located at the zeolite/binder interface (1,3,5 triisopropylbenzene dealkylation).

## EXPERIMENTAL SECTION

### Materials and Preparation

Y (LZY-64 supplied by UOP) and USY zeolites (CBV720 and CBV760 purchased from Zeolyst and hereinafter referred to as USY-1 and USY-2) were used as parent zeolites; their physico-chemical properties are summarized in Table 1. USY-1 and USY-2 are typical of steamed and steamed/acid leached Y zeolites. Their Si/Al ratios range from 2.3 to 28 and they differ by their acidic and textural properties.

Alumina bound zeolite extrudates (dry mass ratio of 30 wt% zeolite and 70 wt% binder, unless otherwise specified) were prepared as follows: 1.7 g of zeolite powder, 0.08 g of Methocel (F4M, Dow Chemicals) and 4.8 g of alkali-free pseudo-boehmite (Catapal B) were mixed and homogenized. Deionized water (4 g) was then added dropwise to the solid mixture to obtain a dough ready for extrusion. The dough was then transferred to a hand extruder (MAKIN's USA Professional Ultimate Clay Gun Extruder) for shaping through a 1.6 mm diameter die. The green extrudates were dried at 323 K for 2 hours in a convection oven and thereafter transferred to a muffle oven where they were calcined as follows: i) 363 K for 12 hours ii) 823 K for 4 hours at with a heating rate of 5 K /min. The calcined extrudates were then recovered, crushed, sieved and the 200-500 µm fraction retained. The parent zeolite powders were heated under identical conditions and used as references.

### Characterization

The crystallinity was determined by X-Ray diffraction (XRD) with a PANanalytical, X'Pert Pro MPD X-ray diffractometer in the 2θ range 3-60º with scanning steps of 0.0167º s-1. To determine the unit cell parameter, the diffraction patterns were indexed and refined using Werner's indexing method (TREOR 90) to a ($Fd\bar{3}m$) symmetry. The Si/Al ratio was then estimated using the Breck-Flanigen equation: Si/Al= (192/(115.2 x (a-24.191)))-1.[33]

$^{27}Al$ and $^{29}Si$ solid state NMR spectra were recorded on a Bruker Avance-400 (magnetic field of 9.4 T) spectrometer using 4 mm rotors. All $^{29}Si$ MAS NMR spectra were recorded with a pulse length of 4 µs (30° flip angle) and a repetition time of 20 s. The $^{27}Al$ MAS NMR spectra were recorded with a pulse length of 2.2 µs (π/12 flip angle) and a recycle delay of 1 s. All MAS NMR experiments were performed using a sample spinning speed of 12 kHz.

A Micromeritics 2020 ASAP gas adsorption analyzer was used for nitrogen sorption measurements. Prior to analysis, the samples were outgassed at 373 K for 1 h and 623 K for 10 h. Specific surface areas were determined from the BET equation. The total pore volume is the nitrogen volume adsorbed at P/P° = 0.99. The t-plot method was used to distinguish the micropores from the mesopores in the samples. The particle size distribution (PSD) was derived from the desorption branch of the $N_2$ isotherm using the Barrett-Joyner-Halenda (BJH) procedure.

The acidic properties of the catalysts were determined by IR spectroscopy of adsorbed pyridine and CO. For pyridine, a conventional glass cell was used, while for CO, a low temperature cell was selected. The latter cell was equipped with $CaF_2$ windows and cooled with liquid nitrogen. Infrared spectra were recorded on a Nicolet Magna 550-FT-IR spectrometer at 2 cm-1 optical resolution. Prior to the measurements, the catalysts were pressed into self-supporting discs (diameter: 1.6 cm, 20 mg $cm^2$) and pretreated in-situ under vacuum ($10^{-6}$ Torr) at 823 K (2 K /min) for 5 h. Pyridine was adsorbed at 373 K. After establishing a pressure of 1 Torr at equilibrium, the cell was evacuated at 523 K to remove the physisorbed species. The amount of pyridine adsorbed on the Brønsted (1545 $cm^{-1}$) and Lewis (1454 $cm^{-1}$) sites was determined by integrating their respective band areas using the following extinction coefficients: ε(B)1545 = 1.35 and ε(L)1454 = 1.5 $cm.mol^{-1}$ for Py.[34] The accessibility indices (ACI) for pyridine, were calculated as describe above.

For CO-adsorption, the sample, activated in an in-situ IR cell, was first cooled to 100 K under vacuum, the cell then filled with 30 torr of Helium to insure high thermal conductivity; small doses (0.5-10 µmol) of CO were then introduced and IR spectra recorded after each dose.

Thermal analyses were performed in an α-alumina crucible on a SETARAM Setsys Evolution system, with air flow of 40 ml/min and a heating rate of 5 K/min.

**Catalytic Probe Reactions**

The catalytic consequences of zeolite binding may be assessed in two reactions: *i)* hydroconversion of n-octane ([n-$C_8$], kinetic diameter 0.43 nm)[35] *ii)* dealkylation of 1,3,5 triisopropylbenzene (TiPBz, kinetic diameter 0.95 nm). The latter, a bulky molecule probes specifically the external and mesoporous surfaces of most zeolites, while n-$C_8$ penetrates all microporosity and reacts also on the external surface.

*i) hydroconversion of n-$C_8$ on derived bifunctional catalysts (Pt/zeolite with Pt = 0.5 wt %).* Catalytic performance was measured at constant temperature and pressure (543 K and 50 bars, $P_{H2}$ = 10 bars) and the space time kept constant (W/F° = 3.2 $kg_{zeol}{\cdot}h{\cdot}mol^{-1}$). The platinum loading (0.5 wt% Pt) on the zeolites was carried out by incipient wetness impregnation with aqueous $Pt(NH_3)_4Cl_2$. The extrudates were then prepared as described above. The reaction takes place in a continuous-flow fixed-bed micro-reactor containing 150 mg of the catalyst diluted with 850 mg of silicon carbide. Prior to testing, all catalysts were calcined *in-situ* at atmospheric pressure for 2 h with flowing dry air at 673 K and then cooled to 573 K under a He flow. The samples were subsequently reduced at 543 K in flowing $H_2$ for 1 h prior to pressurization. All gases were purified from water and oxygen contaminants using 3A zeolite and BTS (Fluka) traps. The feed was delivered by a Gilson 302 liquid chromatography pump. The gaseous products were analyzed online with a Varian 3800 gas chromatograph fitted with a fused silica capillary column (CP-SIL 5 CB Low Bleed/MS) and a flame ionization detector. To avoid transport limitations, all extrudates were crushed/sieved and the 200-500 µm fractions retained for the catalytic tests.

*ii) dealkylation of TiPBz*.[36] The reaction was carried out in a continuous-flow fixed-bed micro-reactor. For each experiment, 20 mg of catalyst was loaded and enclosed between two layers of finely ground inert (SiC, 0.25 mm). The samples were activated under a dry-air stream (Flow = 50 mL $min^{-1}$) as follows: *a*) 393 K for 1 h *b*) temperature raised to 723 K with a ramp rate of 2 K /min followed by a 4 h plateau, *c*) cooling down to 573 K under the same flow. Dried and deoxygenated nitrogen was subsequently introduced at 573 K and the reactor was then cooled to the reaction temperature (493 K). A stream of $N_2$ (400 mL $min^{-1}$) was diverted to a saturator filled with TiPBz (Alfa Aesar, 95 % purity) kept at 344 K ($P_{TiBz}$ = 180 Pa). The total pressure in the reactor was $1x10^5$ Pa and the space time was kept constant (W/F° = 29 $kg_{zeol}.h.mol^{-1}$). The effluent was sampled after 5 min on stream and analyzed on-line by gas chromatography (Varian Cp 3800; HP-PONA 50 m, 0.2 mm, 0.5 µm column, FID detector). To avoid transport disguise of the catalytic results, all extrudates were crushed/sieved and the 200-500 µm fraction retained for catalytic testing; the zeolite powders and mechanical mixtures (70% alumina and 30 % zeolite) were pelletized, crushed and sieved to retain the 200-500 µm fraction.

## Results and discussion

### 1. Physicochemical properties of the parent zeolite powders

Table 1 summarizes key physicochemical properties of the zeolite powders. As expected, the USY's display higher external surface areas than ion exchanged Y prior to the stabilization treatment. The number of Brønsted acid sites, determined by pyridine adsorption, is also different for the three samples: Y has six times more Brønsted sites than the USY's. The accessibility index (ACI) of these sites to pyridine is determined by IR and MAS $^{29}$Si NMR spectroscopy. It is defined as the number of Brønsted acidic sites titrated by pyridine divided by the number of tetrahedral aluminum determined by $^{29}$Si MAS NMR spectroscopy.[37] USY-2 shows the highest ACI (0.6) followed by USY-1 (0.5) and FAU-Y (0.45). The fact that more acid sites are accessible to pyridine on severely treated FAU by biased treatments consisting of selective Al extraction during the steaming of Y to yield USY-1 and further acid leaching of USY-1 leading to USY-2 is in line with the recent observation that sodalite cages can be opened by means of an unbiased (Si, Al) $NH_4F$ leaching of tetrahedral atoms.[38] The crystallinity, calculated using Y as a reference, is about 70 % for both USY. This is mainly due to amorphisation and/or mesopore creation during the hydrothermal and acid leaching treatments.

**Table 1.** Physico-chemical properties of the parent zeolite powders

| Zeolite | **Y** | **USY-1** | **USY-2** |
|---|---|---|---|
| **Unit cell (Å)** [a] | 24.7 | 24.3 | 24.2 |
| **Si/Al** [29 b] | 2.3 | 16 | 28 |
| **$V_{Micro}$ ($cm^3/g$)** [c] | 0.34 | 0.27 | 0.27 |
| **$S_{BET}$ ($m^2/g$)** [c] | 754 | 840 | 805 |
| **$S_{Meso}$ ($m^2/g$)** [c] | 60 | 267 | 261 |
| **Brønsted acidity (µmol/g)** [d] | 1319 | 272 | 239 |
| **Lewis acidity (µmol/g)** [d] | 45 | 104 | 84 |
| **Accessibility index (ACI)** [e] | 0.40 | 0.51 | 0.60 |
| **Crystallinity (%)** [f] | 100 | 71 | 64 |

[a]: refined unit cell parameter [b]: determined by deconvolution of $^{29}$Si MAS NMR spectra, [c]: determined by nitrogen sorption analyses [d]: determined by pyridine adsorption $\varepsilon_{Brønsted}$ at 1550 $cm^{-1}$ =1.35 $cm.\mu mol^{-1}$, $\varepsilon_{Lewis}$ at 1450 $cm^{-1}$=1.5 $cm.\mu mol^{-1}$, [e]: ACI=Number of Brønsted acid sites determined by Pyridine/ Number of framework aluminum estimated by $^{29}$Si NMR, [f]: FAU-Y as 100 % pure crystalline phase.

### 2.SEM and XRD

A representative SEM micrograph of a calcined USY-2 extrudate is displayed in Figure 2. It is dense and homogeneous with a diameter of about 1.5 mm (Figure 2 a) and consists of zeolite aggregates homogeneously dispersed in the alumina matrix (Figure 2 b). All extrudates have a similar appearance. Comparison of the XRD patterns of zeolite Y extrudates (30 wt% zeolite and 70 wt% alumina) and pure Y powder treated under the same conditions (Figure 3), demonstrates that the pseudo-boehmite is fully converted to γ-alumina since no peaks assignable to pseudoboehmite are present. Table 2 lists the XRD-derived lattice parameters and crystallinities of all samples along with the calculated Si/Al ratio using the Breck-Flanigen correlation.[39] After calcination at 823 K, the framework Si/Al ratio of the Y powder, Y*, and its extrudates, Y/Ext, both increase to 3. The crystallinity of Y* and its derived extrudates both decrease to about 70 %. On the other hand, USY-1 and USY-2 extrudates keep the same Si/Al ratio and crystallinity as their parents. This is expected as USY's have already been steam-stabilized and will not evolve under such relatively mild calcination conditions.

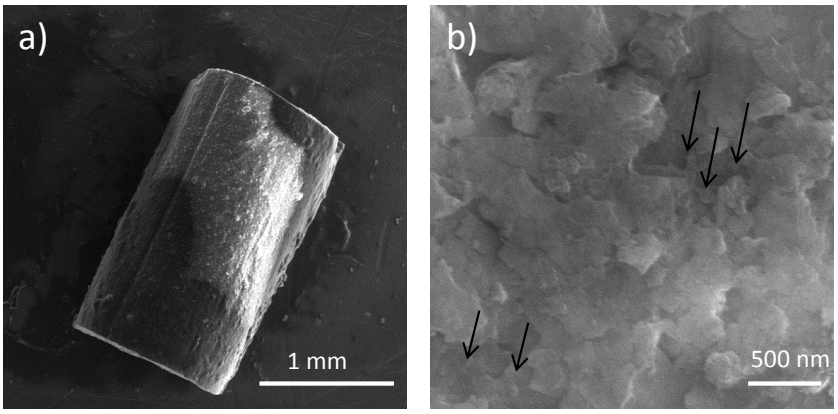


**Figure 2.** Representative SEM micrographs of USY-2 extrudates a) overall view b) zoom on zeolite particles (arrows).

**Table 2.** Unit cell parameters, Si/Al ratio, and crystallinities of zeolite powders and their derived extrudates (30 wt% zeolite - 70 wt% alumina).

| Samples | Unit cell (Å) | Si/Al[a] | Crystallinity (%) |
|---|---|---|---|
| Y | 24.69 | 2 | 100 |
| Y* | 24.62 | 3 | 76 |
| Y/Ext | 24.62 | 3 | 70 |
| USY-1 | 24.30 | 14 | 71 |
| USY-1* | 24.30 | 14 | 69 |
| USY-1/Ext | 24.30 | 14 | 70 |
| USY-2 | 24.25 | 27 | 74 |
| USY-2* | 24.25 | 27 | 66 |
| USY-2/Ext | 24.25 | 27 | 67 |

[a] Breck-Flanigen correlation: Si/Al= (192/(115.2 x (a-24.191))-1; a is the unit cell parameter

* Zeolite calcined at 823 K.

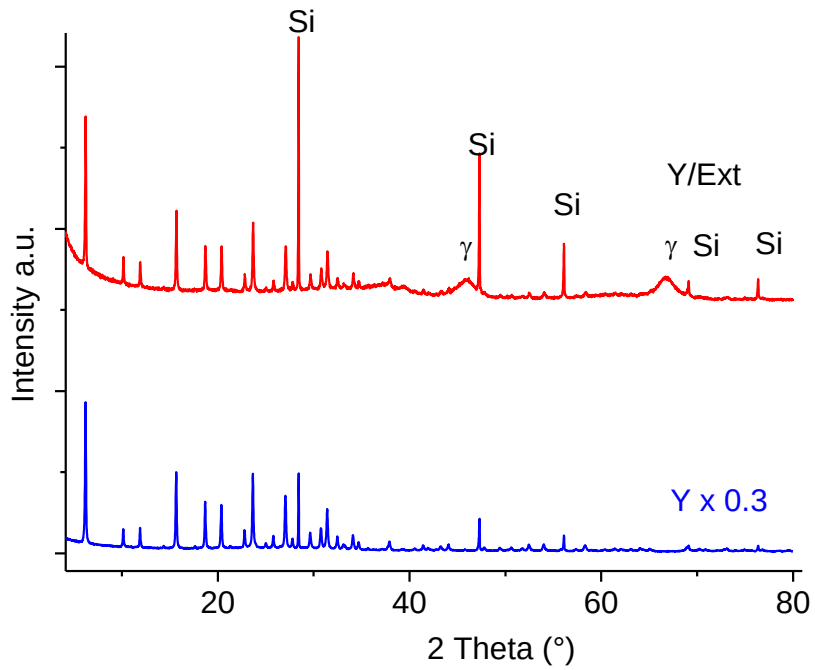


**Figure 3.** XRD patterns: *top* Y extrudates (30 wt% zeolite) *bottom* Y* powder, both after thermal treatment at 823 K (scaled to 30%). The sharp Si peaks belong to the internal standard used for unit cell measurement while γ indicates peaks characteristic of γ-$Al_2O_3$.

**3. Nitrogen physisorption**

Nitrogen sorption isotherms of Y and USY-2 (30 wt% zeolite, 70 wt% γ-$Al_2O_3$) zeolite extrudates show a micropore volume of 30 % of their parent zeolite, indicating that no pore blockage or filling occurs during extrusion, Table SI.1. Their total pore volume is higher than the sum of the components taken separately and could be due to additional porosity at the zeolite-binder interface. The extrudates display Type IV isotherms with a combination of two H4 hysteresis loops (Figure 4 a-b). The first hysteresis, similar to that of pure alumina, corresponds to the native mesoporosity of the alumina binder while the second, observed at higher relative pressure ($P/P^\circ > 0.7$,) may be related to additional pores created at the zeolite-binder interface; similar results are obtained for the USY-1. The corresponding pore-size distributions are shown in Figure 4 c-d). Both zeolite extrudates (Y/Ext and USY-2/ Ext) have a wider pore-size distribution than the zeolite powders and the alumina. The additional mesoporosity is in the range 10-20 nm.

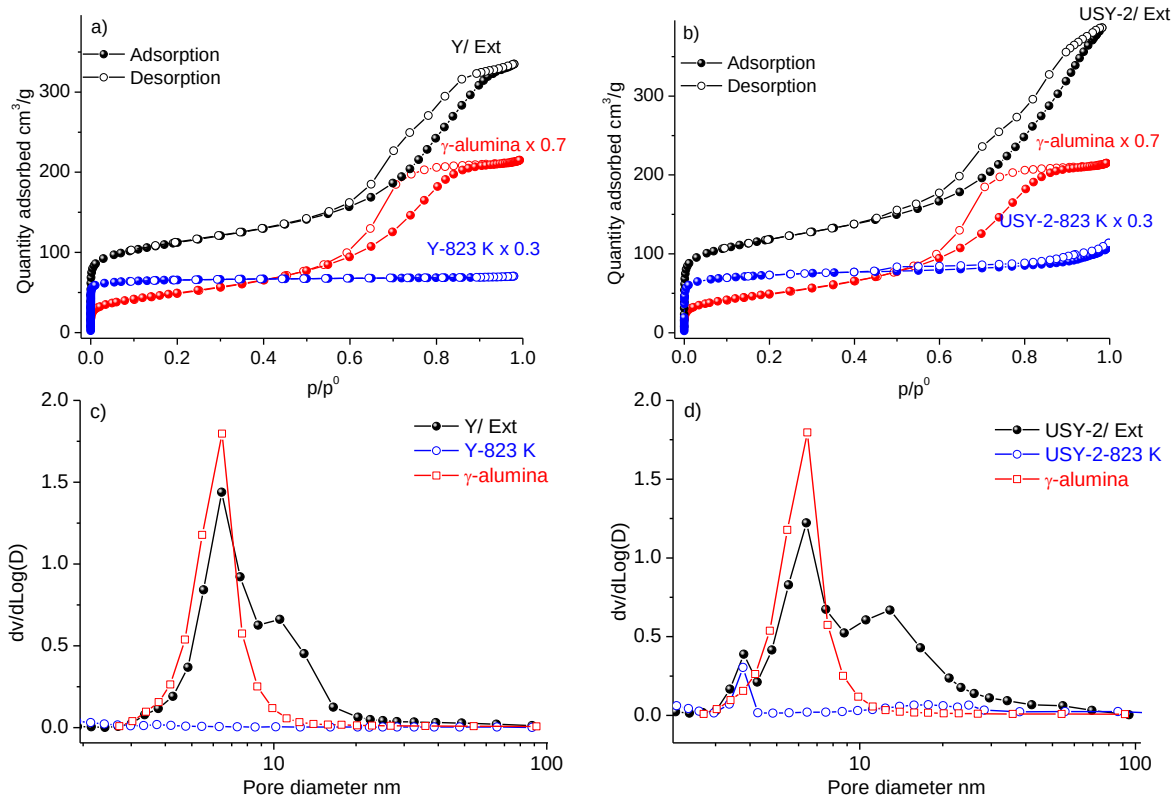


**Figure 4.** Nitrogen sorption isotherms and derived (BJH) pore size distributions a-c) Y, Y extrudates and γ-$Al_2O_3$, calcined at 823 K, b-d) USY-2, USY-2 extrudates and γ-$Al_2O_3$ calcined at 823 K.

**4. Thermal Analysis (TG/DSC)**

The TG/DSC of pure zeolites (Y and USY-2), pure pseudoboehmite (Catapal B) and green extrudates (30 wt% zeolite [Y or USY-2], 70 wt% Catapal B) dried at 323 K for 2 hours are reported at Figure 5. The thermograms of the pure zeolites and pseudoboehmite are normalized to their respective concentration in the extrudates. The weight loss (TG) and associated thermal effects (DSC) of green extrudates (Y and USY-2) take place mainly in three steps:

the first weight loss (~ 15 w%), below 500 K, is the removal of physisorbed water (30 w% from the zeolite and 70 w% from pseudoboehmite)

the phase transition of pseudo-boehmite to γ-$Al_2O_3$ takes place around 700 K with an associated weight loss of 13 w% (70 w% of pure pseudoboehmite)[40,41]

the third weight loss (~ 3 w% and 5 w% between 500 K-620 K) for green Y and USY-2 extrudates is due to the Methocel (1%) combustion.

These weight losses are accompanied by one endotherm at *ca.* 380 K (water desorption), one exotherm at 500 K and at least two endotherms at 550 and 620 K. The exotherm corresponds to the Methocel combustion, while the endotherms correspond to the dehydroxylation processes. These signals are absent from the parent zeolite and pseudoboehmite treated under the same conditions, indicating that some zeolite-binder interaction takes place between 500 – 650 K; its exact nature needs to be determined, *vide infra*.

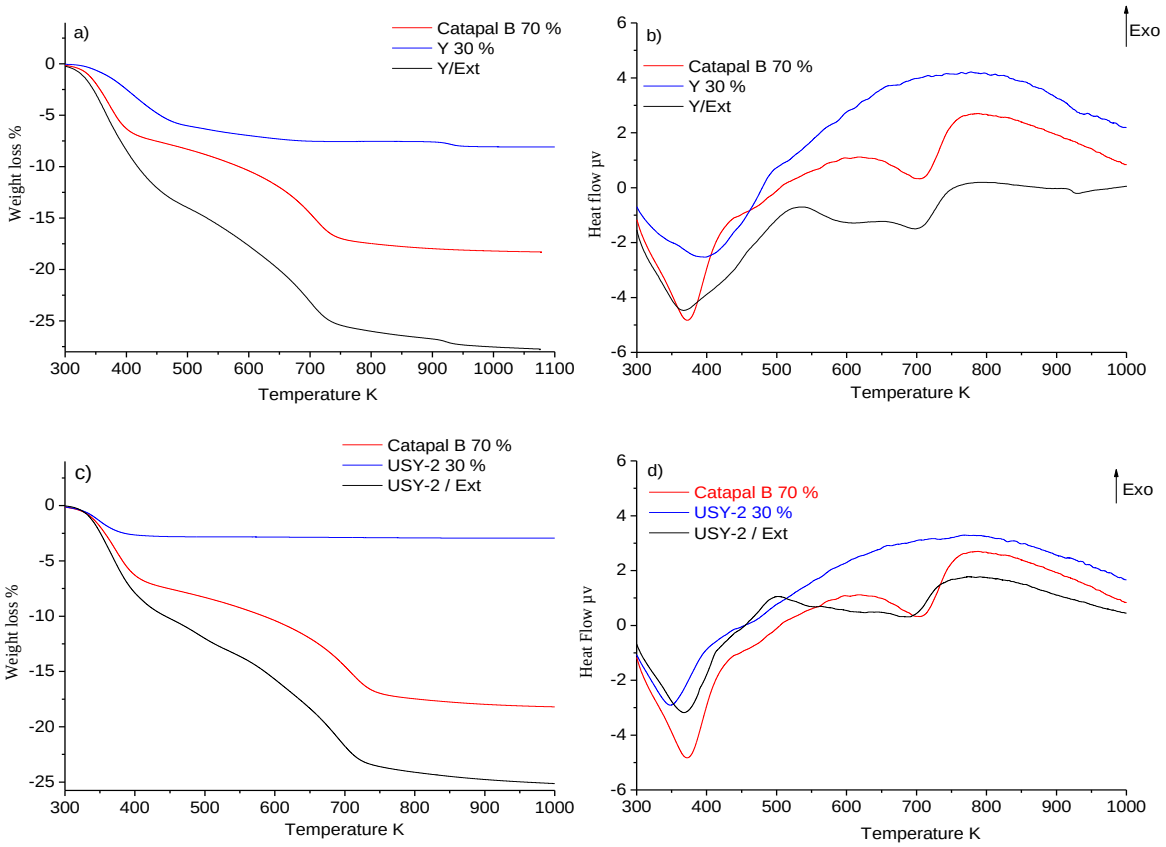


**Figure 5**. TG/DSC thermograms of (a-b) Catapal B, zeolite Y and green extrudates 30 wt% Y zeolite, 70 wt% Pseudoboehmite (dried at 323 K for 2 hours), c-d) Catapal B, zeolite USY-2 and green extrudates 30 wt% USY-2 zeolite-70 wt% Pseudoboehmite (dried at 323 K for 2 hours).

## 5. $^{27}$Al NMR Spectroscopy

$^{27}$Al NMR spectroscopy can determine the distribution of framework (tetrahedral and distorted tetrahedral) and extra-framework aluminum (octahedral and pentahedral) and to identify features of the various forms of alumina. [42]

The $^{27}$Al NMR spectra of the Y zeolite powder and its derived green (dried at 323 K) and calcined (623 K and 823 K) extrudates (30 wt% Y zeolite, 70 wt% pseudoboehmite) are compared in Figure 6A-B). No spectral features that may be attributed to zeolite-binder interactions can be found as all peaks are located in similar regions of the NMR spectra.

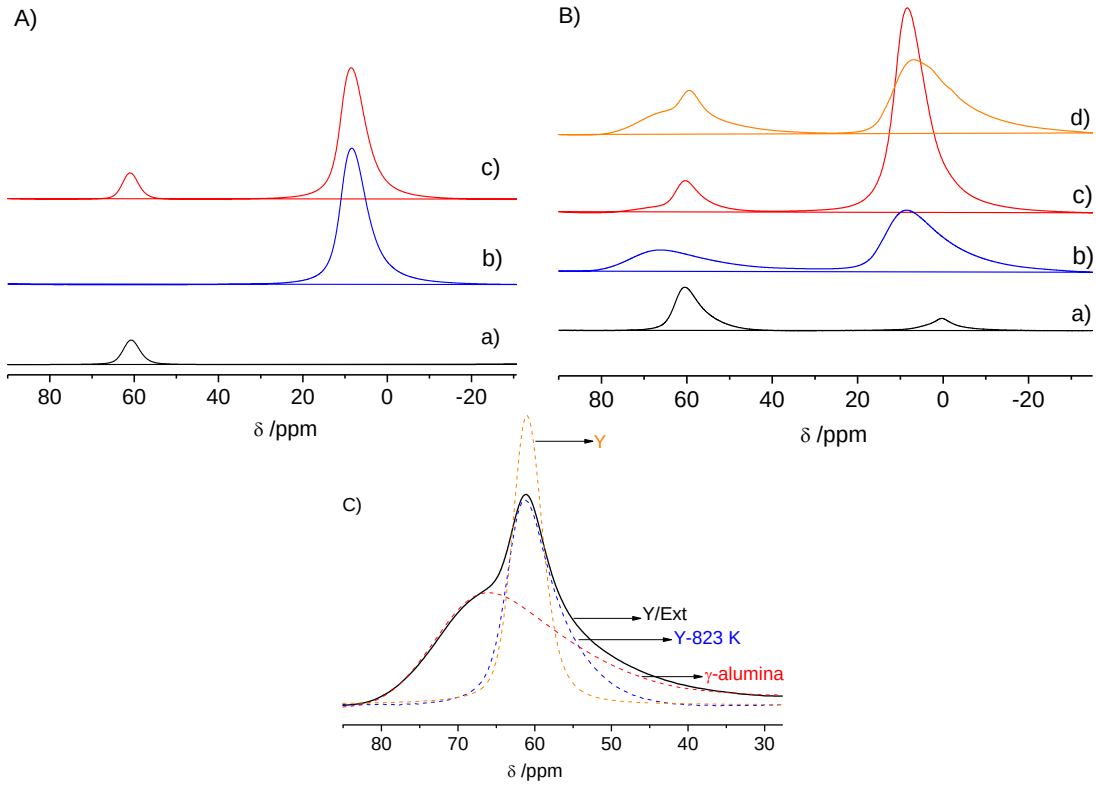


**Figure 6.** A) $^{27}$Al MAS NMR spectra of *a*) Y, *b*) pseudoboehmite, c) green Y extrudates (dried at 323 K), B) $^{27}$Al MAS NMR spectra of a) Y calcined at 823 K, *b*) γ-alumina, *c*) calcined Y extrudates (623 K), *d*) calcined Y extrudates (823 K), C) zoom on the 60 ppm region.

Figure 6 C) highlights a broad tetrahedral signal in Y/Ext made of two peaks around 70 and 60 ppm; the first is typical of tetrahedrally coordinated aluminum in a spinel structure ($\gamma$–$Al_2O_3$) while the second can be attributed to tetrahedral aluminum in a Y zeolite. A broad resonance in the 50-40 ppm range indicates the presence of distorted tetrahedral or pentacoordinated Al but interferes with the γ-alumina resonance; the same holds for the parent zeolite Y after heating.

The amount of zeolitic tetrahedral Al in extrudates is apparently similar to its parent powder calcined under the same temperature, (Figure 6 C) in agreement with the XRD data (Table 2). The octahedral aluminum in the zeolite powder (0 ppm, corresponding to monomeric $Al^{+3}$, Figure 6 B a) almost disappears after extrusion and may be masked by a new broader peak around 10 ppm (Figure 6 B c) due to the binder. These preliminary qualitative results indicate that conventional $^{27}$Al NMR techniques are not able to resolve the intricate distribution of Al species in this complex system and may imply that some Al is in such distorted environments it cannot be probed without resorting to more advanced NMR techniques (spectral editing, MQ-MAS, DNP…) to provide more relevant information.[43] IR spectroscopy of specific probes and catalytic testing with reactants of different sizes could shed more light on the nature and location of the zeolite-binder interactions suggested by TG/DSC.

## 6. Acidity monitored by IR spectroscopy

### 6.1. Pyridine Adsorption

Pyridine adsorption monitored by infrared spectroscopy is customarily utilized to assess acidic properties (Brønsted, BAS and Lewis, LAS) of zeolite powders. Figure 7a) shows the infrared spectra of zeolite Y and USY-2 after activation at 723 K under vacuum. Three bands appear in the OH region: *i)* 3745 $cm^{-1}$: silanol groups, more

intense in USY-2 than in Y as dealumination and stabilization leads to Si-OH formation, *ii)* 3640 $cm^{-1}$ and 3545 $cm^{-1}$: bridging hydroxyls located in supercages and sodalite cages, respectively. Using molar absorption coefficients ($\varepsilon_{HF}$ = 6.76 $cm.mol^{-1}$ and $\varepsilon_{LF}$ = 5.3 $cm.mol^{-1}$) from our group,[34] we estimate acid site concentration in the supercages at 1295 µmol/g (38 %) and in the sodalite cages at 2090 µmol/g (62 %), in agreement with the literature.[44] USY-2 shows two additional shoulders at 3625 and 3560 $cm^{-1}$ usually assigned to BAS perturbed by extra-framework aluminum.

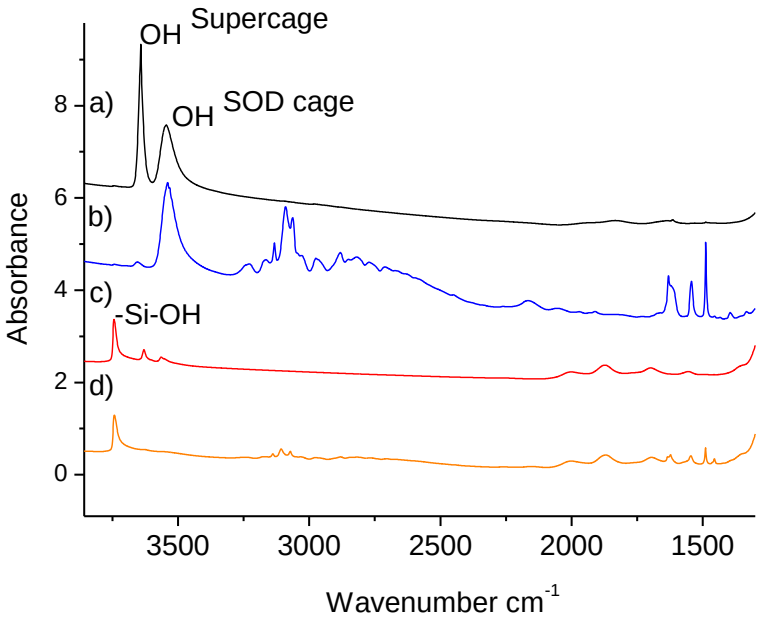


**Figure 7.** IR spectra of Y *a*) after activation at 723 K, *b*) after pyridine adsorption and evacuation under secondary vacuum at 523 K, *c*) USY-2 powders after activation at 723 K, *d*) after pyridine adsorption and evacuation under secondary vacuum at 523 K.

After pyridine adsorption on the Y zeolite, the BAS at 3640 cm-1 (supercages) disappear entirely while those at 3545 cm-1 (sodalite cages) do not change. Only a broadening of the 3545 cm-1 band is observed due to a long-range perturbation, Figure 7a-b). In USY-2, the 3640 cm-1 and 3545 cm-1 bands disappear after pyridine adsorption, Figures 7c-d). The acid site concentrations in zeolite powders and extrudates, using the two bands characteristic of Brønsted (1545 cm-1) and Lewis acid sites (1450 cm-1) are given in Table 3, where bracketed concentrations represent extrapolation to 100% zeolite, i.e. no binder. The BAS concentration sharply decreases after calcination while that of Lewis acid sites increases due to dealumination, a well-known behavior of Y zeolites. The Brønsted acidity of USY-2 does not change after heating as this zeolite is already well stabilized while its Lewis acidity increases due to a reorganization of extra-framework aluminum species.

It is notable that the concentration of BAS in extruded zeolites is systematically higher than in their parent: BAS in Y/Ext are 29 % higher and 8 % in USY-2/Ext. The framework Si/Al (Table 2) are identical for Y and its extrudates and their 27Al NMR spectra show only minor changes in tetrahedral Al while more changes are apparent in the octahedral region. This could indicate the presence of a new phase resulting from interactions between the zeolite and its alumina binder. The formation of an amorphous silica alumina (ASA) phase may be invoked, but cannot be proven based on the evidence collected so far. This hypothesis can be further investigated by CO adsorption monitored by IR spectroscopy.45

**Table 3.** Acidic properties of γ-alumina, zeolite powders and their derived extrudates determined by pyridine adsorption

| Sample | Brønsted[a] µmol/g | Lewis[b] µmol/g |
|---|---|---|
| γ-alumina | / | 370 |
| Y | 1320 | 47 |
| Y* | 203 | 703 |
| Y/ Ext | 78 (260)** | 304 |
| USY-2 | 216 | 67 |
| USY-2* | 213 | 153 |
| USY-2 /Ext | 69 (230)** | 335 |

a: $\varepsilon_{\text{Brønsted sites}}$ at 1550 $cm^{-1}$ =1.3 $cm.\mu mol^{-1}$, b: $\varepsilon_{\text{Lewis sites}}$ at 1450 $cm^{-1}$ = 1.5 $cm.\mu mol^{-1}$.

* calcination at 823 K

** bracketed numbers: extrapolated to 100 % zeolite.

### 6.2. CO Adsorption

CO is a weak base with a small kinetic diameter (0.376 nm) and its stretching frequency, ν(CO) observed by IR, is very sensitive to the strength of acid sites, BAS and LAS, when adsorbed at low temperature (T ≈ 100 K). For strong LAS, ν(CO) is 2230 $cm^{-1}$ and shifts to 2157 $cm^{-1}$ for weaker sites while for BAS, the range lies between 2180 and 2152 $cm^{-1}$. Correlating the ν(CO) with ν(OH) (3000-3700 $cm^{-1}$) band shifts allows to distinguish coordinated from H-bonded CO. Moreover, the shift of the ν(OH) upon CO adsorption, Δν(OH), is proportional to the strength of BAS; the ν(CO) frequencies and Δν(OH) are therefore good indicators of the acidic strength of the OH groups. [46]

The stepwise adsorption of small CO doses at 100 K, up to saturation, monitors the acidity developed on Y zeolite, its derived extrudates (Y-Ext) and γ-alumina. All IR spectra are compared at full CO saturation and normalized to an identical zeolite content. Figure 8 reports the difference spectra, *i.e.* the spectra of an activated (823 K) sample is subtracted from its spectra after CO addition; positive absorbances indicate the appearance of new peaks while negative ones witness a disappearance.

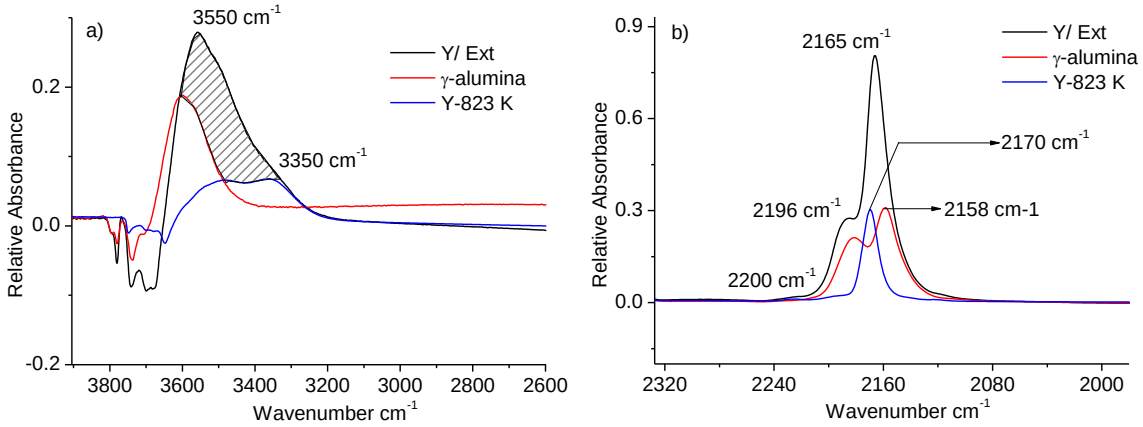

**Figure 8**. Difference spectra (spectra of the activated sample subtracted from its spectra after CO saturation) on Y, Y/Ext and γ-alumina (calcination at 823 K), *a*) OH region *b*) CO region. The dashed area in *a*) shows the appearance, on the extrudates, of a new band associated with acid sites of intermediate acidic strength.

Upon CO adsorption on γ-$Al_2O_3$, the intensity of its OH bands (3700-3800 $cm^{-1}$) decreases with a simultaneous appearance of a broad OH band at lower wavenumbers (3600-3550 $cm^{-1}$), Figure 8a. Meanwhile, in the ν(CO) region two distinct bands appear at 2190 and 2160 $cm^{-1}$ commonly assigned to medium strength LAS and weak BAS, respectively, Figure 8b.[46]

Upon CO adsorption on zeolite Y, the intensity of the bridging hydroxyls (3650 $cm^{-1}$) decreases while two OH bands appear at 3350 and 3450 $cm^{-1}$. The corresponding Δν(OH) are 300 and 200 $cm^{-1}$, respectively, indicative of strong BAS. In the CO region only one band at 2170 $cm^{-1}$ increases upon CO adsorption.

In the case of Y/Ext, the OH bands shift upon CO adsorption and at least three perturbed BAS differing by their acid strengths appear:

1- High: as observed in Y with Δν(OH) of 300 - 200 $cm^{-1}$ and ν(CO) at 2170 $cm^{-1}$.

2- Low: as observed in γ-alumina with ν(CO) at 2160 $cm^{-1}$.

3- Intermediate (dashed area in Figure 8a): perturbed OH groups with a ν(OH) in the region 3450-3500 $cm^{-1}$. The ν(CO) are in the range 2165 $cm^{-1}$ - 2190 $cm^{-1}$; such a Brønsted acidity is observed in ASA. [46, 47]

The important conclusion is that, in addition to the strong BAS of the zeolite and the weak BAS of alumina, Y/Ext displays new BAS. They bear the characteristics of ASA and are most probably generated during the pseudoboehmite transformation to γ-$Al_2O_3$ transformation of extrudates, *vide supra*. It remains valuable in the future to probe their accessibility, *i.e.* their location either in micropores or in a less confined environment such as the external surface of the zeolite, *vide infra*.

**7. Catalytic Probe Reactions**

The catalytic performances of zeolite powders and their extrudates are first assessed in the hydro-isomerization of n-$C_8$, a molecule accessing all acid sites in the FAU structure except those in closed sodalite cages. The addition of a hydrogenation function, Pt, promotes a bifunctional reaction mechanism and minimizes deactivation during catalytic testing. Figure 9 shows the n-$C_8$ conversion on Pt/USY-2 and its derived extrudates, Pt/USY-2/Ext. Both display close conversions and selectivities (Table SI.2.), the extrudates being marginally but systematically more active. A similar trend is observed for Pt/Y, Pt/USY-1 and their derived extrudates.

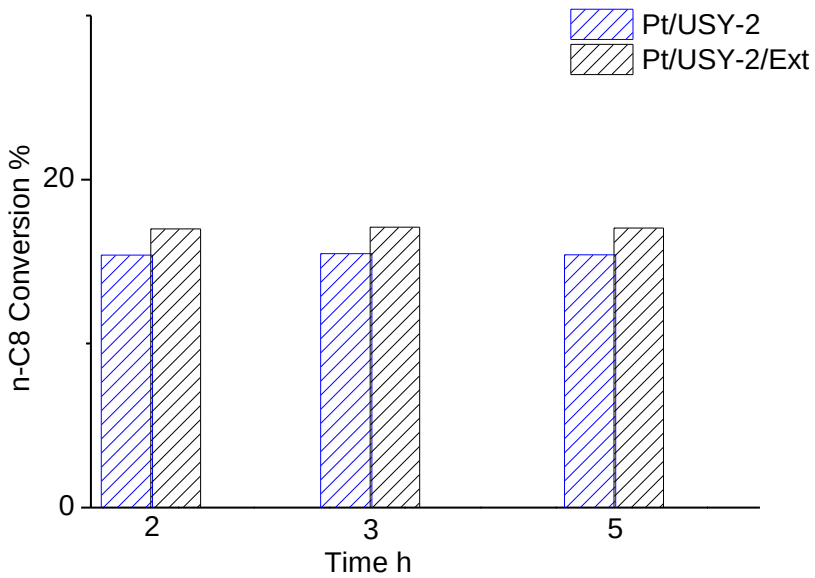

**Figure 9**. n-$C_8$ hydroconversion on Pt/USY-2 and its derived extrudates, Pt/USY-2/Ext (calcined at 823 K) at three different times on stream (T = 543 K P = 50 bar, $P_{H2}$ = 10 bar, W/F° = 3.2 $kg_{zeol}$·h·$mol^{-1}$).

1,3,5 Tri-isopropyl benzene (TiPBz) dealkylation probes only the external and mesoporous zeolite surfaces, including the large pore FAU (Y) structure; it is a bulky molecule (0.95 nm) too large to penetrate FAU micropores. Physical mixtures of 30 wt % zeolites (Y and USY-2 calcined at 823 K) and 70 wt% γ-alumina are also tested for comparative purposes. Figure 10 a-b) shows the catalytic conversion at different time on stream for the parent zeolites, their extrudates and physical mixtures of the parent zeolite and its binder; further details are provided in Table SI.3. While the physical mixtures and their parent zeolites (Y, USY-1 and USY-2) behave similarly, their (Y and USY-2) extrudates are significantly more active at similar zeolite contents. These results agree with the IR and TG/DSC characterization and further indicate that the additional acidity created during the extrusion process is accessible to a bulky molecule. This also implies that these new catalytic sites are most probably located at the interface between the zeolite and its binder and not inside the zeolite microporosity.

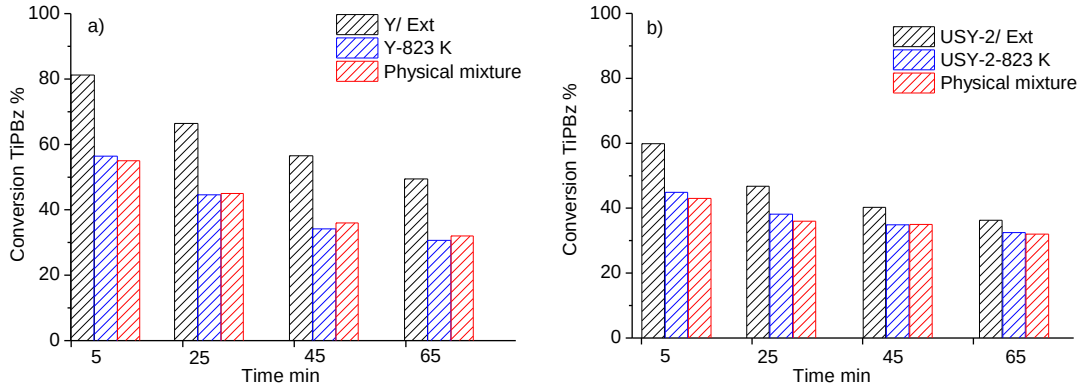


**Figure 10.** TiPBz conversion (T = 493 K, W/F° = 29 $kg_{zeol}$.h.$mol^{-1}$) at different time on stream *a)* Y/Ext, Y, physical mixture Y (30 wt%)/γ-$Al_2O_3$ (70 wt%) *b)* USY-2/Ext, USY-2, physical mixture USY-2 (30 wt%)/γ-$Al_2O_3$ (70 wt%). All samples calcined at 823 K.

USY-1/Ext with two different zeolite/binder ratios, 50/50 and 30/70, and their parent USY-1 are also compared in the TiPBz dealkylation, Figure 11. Again, all extrudates are more active than their parent zeolites calcined at the same temperature (823 K). Moreover, extrudates with a higher alumina (70 wt%) content are more active, on an equal zeolite basis, than those with 50 wt% alumina. The fact that zeolite "dilution" in a binder increases its activity, at first sight counterintuitive, emphasizes the importance of understanding and controlling the zeolite binder interactions as this increased catalytic activity is due to more aluminum species leaving the binder to interact with the zeolite and form a new easily accessible active phase .[28]

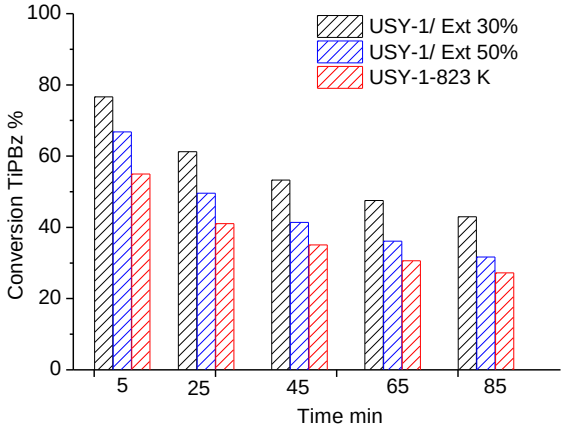

**Figure 11.** TiPBz conversion (T = 493 K, W/F° = 29 $kg_{zeol}.h.mol^{-1}$) as a function of time on stream for USY-1 extrudates (30 %w and 50 %wt zeolite) and their USY-1 parent (823 K calcined).

## Conclusions

Alumina-bound extrudates derived from LZY-64 (Y), CBV 720 (USY-1) and CBV 760 (USY-2) zeolites were prepared with pseudoboehmite. After calcination of the green extrudates, XRD and $^{27}$Al NMR indicate that all extruded zeolites keep the framework Si/Al ratio and crystallinity of their parent calcined under similar conditions while additional mesoporosity is provided by the binder. However, all extrudates contain more Brønsted acid sites (pyridine adsorption monitored by IR) than their parent zeolites. This added acidity is attributed to newly created acid sites, reminiscent of amorphous silica-alumina (CO adsorption monitored by IR) not located in the zeolite micropores (1,3,5 TiPBz dealkylation). These chemical reactions between a zeolite and its binder take place during the calcination of the green extrudates (TG/DSC), when pseudoboehmite (all Al in 6-fold coordination) is converted to $\gamma$-$Al_2O_3$ (Al in 6-, 4- and 5-fold coordination), releasing water that in turn promotes the mobility of aluminum species.

The significant increase in catalytic performances of the extrudates in the conversion of a bulky molecule, TiPBz, compared to their parent zeolites and physical mixtures of zeolites and their binders indicates that the newly created catalytic sites are not located in the zeolite micropores but near their external surface.

We demonstrate that, although zeolite-binder interactions are difficult to assess with standard zeolite characterization techniques, others such as IR of specific probe molecules yield important informations and provide insight in the nature and location of such chemical interactions. Binding FAU zeolite powders with pseudo-boehmite can lead to catalysts where important changes in the quality and quantity of active sites take place. More advanced characterization and control of this important step, would provide great value when zeolite-based catalysts and adsorbents move from the laboratory to a commercialization phase as it would help clearly describe the nature and location of the chemical interactions observed on extrudates. For future work, advanced NMR techniques (2D MQ-MAS, DNP…) as well as high resolution visualization techniques should shed deeper insights in the interaction between a zeolite and its binder. With the increasing use of nanozeolites [36,48] and other zeolites (*e.g.* MWW-structure type) [49,50] whose active sites are located on their external surfaces, zeolite-binder interactions will become ever more relevant and need to be controlled. Optimum utilization of such newly created sites at the interface of zeolite crystallites and their binders will depend on the specific application and the active site requirements for that application. In some cases such as hydrocracking, it is likely that enhanced zeolite-binder interactions would be beneficial, while in other reactions (*e.g.* para-xylene production from toluene alkylation or disproportionation, xylenes and ethylbenzene isomerization…) they should be minimized.[51] As shaping processes, like extrusion, can affect the number and nature of active sites in catalysts, they belong to the post-synthesis modification toolkit enabling the fine-tuning of chemical properties of catalysts or adsorbents. The potential to significantly modify some properties of catalysts (activity, selectivity and stability) and adsorbents should therefore be carefully exploited and built into catalyst and adsorbent design for each targeted application. Deeper insights into this process will lead to better design rules for superior industrial catalysts and therefore deserves the full scientific attention of the academic and industrial communities.

## Acknowledgments

Honeywell UOP for funding and permission to publish

References


1 J. S. J. Hargreaves, and A. L. Munnoch, A survey of the influence of binders in zeolite catalysis. Catal. Sci. Technol 2013, 3, 1165-1171.
2 Mendes, P. S. F.; Silva, J.; Ribeiro, M. F.; Daudin, A.; Bouchy, C. From powder to extrudate zeolite-based bifunctional hydroisomerization catalysts: on preserving zeolite integrity and optimizing Pt location. J. Ind. Eng. Chem. 2018, 62, 72-83.
3 Mitchell, S.; Michels, N. L.; Pérez-Ramírez, J. The curious case of zeolite–clay/binder interactions and their consequences for catalyst preparation. Chem. Soc. Rev. 2013, 42, 6094-6112.
4 Michels, N. L.; Mitchell, S.; Pérez-Ramírez, J. Effects of Binders on the Performance of Shaped Hierarchical MFI Zeolites in Methanol-to-Hydrocarbons. ACS Catal. 2014, 4, 2409−2417.
5 De Jong, K. P.; Zecevic, J.; Friedrich, H.; De Jongh, P. E.; Bulut, M.; Van Donk, S.; Kenmogne, R.; Finiels, A.; Hulea, V.; Fajula, F. Zeolite Y Crystals with Trimodal Porosity as Ideal Hydrocracking Catalysts. Angew. Chem. Int. Ed. 2010, 49, 10074 -10078.
6 Corma, A.; Huber, G. W.; Sauvanaud, L.; O'Connor, P. Biomass to chemicals: Catalytic conversion of glycerol/water mixtures into acrolein, reaction network. J. Catal. 2008, 257, 163–171.
7 Bingre, R.; Louis, B.; Nguyen, P. An Overview on Zeolite Shaping Technology and Solutions to Overcome Diffusion Limitations. Catal. 2018, 163(8), 2-18.
8 Withing, G.T., Chung, S.H., Stosic, D., Chowdhurry, A.D., Van der Wal, L.I., Fu, D., Zecevic, J., Travert, A., Houben, K., Baldus, M., Weckhuysen, B.M. Multiscale mechanistic insights of shaped catalyst body formulations and their impact on catalytic properties. ACS Catal. 2019, 9, 4792-4803.
9 Kraushaar-Czarnetzki, B. Shaping of Solid Catalysts, in Synthesis of Solid Catalysts, K.P. de Jong, ed., Wiley-VCH, 2009, Weinheim, 73-199.
10 Rostrup-Nielsen, J.R. Industrial Relevance of Coking. Catal. Today 1997, 37, 225-232.
11 Moulijn, J.A.; Van Diepen, A.E.; Kapteijn, F. Catalyst Deactivation: is it predictable? What to do. Appl. Catal. A 2001, 212, 3-16.
12 Sie, S.T. Consequences of Catalyst Deactivation for Process Design and Operation. Appl. Catal. A 2001, 212, 129-151.
13 Kubicek, N.; Vaudry, F.; Chiche, B. H.; Hudec, P.; Di Renzo, F.; Schulz, P.; Fajula, F. Stabilization of zeolite beta for FCC application by embedding in amorphous matrix. Applied Catalysis A: General 1998, 175, 159-171.
14 Gélin, P.; Des Courières, T. Role of the amorphous matrix in the hydrothermal ageing of fluid catalytic cracking catalysts. Appl. Catal. 1991, 72, 179–192.
15 Verkleij, S. P.; Whiting, G. T.; Esclapez, S. P.; Mertens, M. M.; Bons, A. J.; Burgers, M.; Weckhuysen, B. M. Operando micro-spectroscopy on ZSM-5 containing extrudates during the oligomerization of 1-hexene. Catal. Sci. Technol. 2018, 8, 2175-2185.
16 Lee, Y. J.; Kim, Y. W.; Viswanadham, N.; Jun, K. W.; Bae, J. W.. Appl. Catal. A 2010, 374, 18-25.
17 Michels, N. L.; Mitchell, S.; Pérez-Ramírez, J. Effects of Binders on the Performance of Shaped Hierarchical MFI Zeolites in Methanol-to-Hydrocarbons. ACS Catal. 2014, 4, 2409-2417.
18 Mitchell, S.; Michels, N. L.; Kunze, K.; Pérez-Ramírez, J. Visualization of hierarchically structured zeolite bodies from macro to nano length scales. Nat. Chem. 2012, 4, 825-831.
19 Schwarz, S.; Kojima, M.; O'Connor, C. T. Effect of stirring, extrusion and pelletisation on high pressure propene oligomerisation and xylene isomerisation over ZSM-5. Appl. Catal. 1991, 68, 81-96.
20 R. L. Bedard, in Zeolites in Industrial Separation and Catalysis, ed. S. Kulprathipanja, Wiley-VCH, Weinheim, Germany, 2010, 61-83.
21 Shihabi, D. S.; Garwood, W. E.; Chu, P.; Miale, J. N.; Lago, R. M.; Chu, C. T. W.; Chang, C. D. Aluminum insertion into high-silica zeolite frameworks: II. Binder activation of high-silica ZSM-5 J. Catal. A 1985, 93, 471-474.
22 Chang, C. D.; Hellring, S. D.; Miale, J. N.; Schmitt, K. D.; Brigandi, P. W.; Wu, E. L.; Insertion of aluminium into high-silica-content zeolite frameworks. Part 3.—Hydrothermal transfer of aluminium from $Al_2O_3$ into [Al]ZSM-5 and [B]ZSM-5. J. Chem. Soc. Faraday Trans. 1 1985, 81, 2215-2224.
23 Noronha, Z. M.; Monteiro, J. L. F.; Gelin, P. The role of matrix embedding on the properties of steamed mordenites. Microporous Mesoporous Mater. 1998, 23, 331-344.
24 Itani, L.; Valtchev, V.; Patarin, J.; Rigolet, S.; Gao, F.; Baudin, G. Centimeter-sized zeolite bodies of intergrown crystals: Preparation, characterization and study of binder evolution. Microporous Mesoporous Mater. 2011, 138, 157-166.
25 Corma, A.; Grande, M.; Fornes, V.; Cartlidge, S. Gas oil cracking at the zeolite-matrix interface. Appl. Catal. 1990, 66, 247-255.
26 De la Puente, G.; Sousa-Aguilar, E. F.; Costa, A. F.; Sedran, U. The influence on selectivity of the aluminum content in the matrix of FCC catalysts. Appl. Catal. A 2003, 242, 381-391.
27 Lucas, A.; Valverde, J. L.; Sanchez, P.; Dorado, F.; Ramos, M. J. Influence of the Binder on the n-Octane Hydroisomerization over Palladium-Containing Zeolite Catalysts. Ind. Eng. Chem. Res. 2004, 43, 8217-8225.
28 Whiting, G. T.; Chowdhury, A. D.; Oord, R.; Paalanen, P.; Weckhuysen, B. M. The curious case of zeolite–clay/binder interactions and their consequences for catalyst preparation. Faraday Discuss 2016, 188, 369-386.
29 Buurmans, I. L. C.; Ruiz-Martínez, J.; Knowles, W. V.; Van Der Beek, D.; Bergwerff, J. A.; Vogt, E. T. C.; Weckhuysen, B. M. Catalytic activity in individual cracking catalyst particles imaged throughout different life stages by selective staining. Nat. Chem. 2011, 3, 862-867.
30 Castaño, P.; Ruiz-Martínez, J.; Epelde, E.; Gayubo, A.G.; Weckhuysen, B. M. Spatial Distribution of Zeolite ZSM-5 within Catalyst Bodies Affects Selectivity and Stability of Methanol-to-Hydrocarbons Conversion. ChemCatChem 2013, 5, 2827-2831.

31 a) Bellussi, G.; Carati, A.; Millini, R. Chapter 16 “Industrial potential of zeolites” in Zeolites and Catalysis: Synthesis, reactions, and Applications, Cejka, J.; Corma, A.; Zones, S.; Wiley-VCH, Weinheim, 2010. b) Kraushaar-Czarnetzki, B.; Muller, S. P. Chapter 9 “Shaping of solid catalysts” in “synthesis of solid catalysts”, De Jong, K. P. Wiley-VCH, Weinheim, 2009. c) Schüth, F.; Hesse, M. Chapter 2 “Preparation of solid catalysts” in Handbook of Heterogeneous Catalysis, Ertl, G.; Knözinger,; Weitkamp,; H. J. Wiley-VCH, Weinheim, 2008. d) Bedard, R. L. Chapter 3 “Synthesis of zeolites and manufacture of zeolitic catalysts and adsorbents” in Zeolites in industrial separation and catalysis, Kulprathipanja, S. Wiley-VCH, Weinheim, 2010. e) Akhtar, F.; Andersson, L.; Ogunwumi, S.; Hedin, N.; Bergstrom, L. Structuring adsorbents and catalysts by processing of porous powders. J. of the European Ceramic Society 2014, 34, 1643-1666.
32 Freiding, J.; Kraushaar-Czarnetzki, B. Novel extruded fixed-bed MTO catalysts with high olefin selectivity and high resistance against coke deactivation. Appl. Catal. A. 2011, 391, 254-260.
33 D. W. Breck, E. M. Flanigen, Molecular Sieves, Society of Chem. Ind. London, 1968, 47-61.
34 Thibault-Starzyk, F.; Gil, B.; Aiello, S.; Chevreau, T.; Gilson, J.-P. In situ thermogravimetry in an infrared spectrometer: an answer to quantitative spectroscopy of adsorbed species on heterogeneous catalysts. Microporous Mesoporous Mater. 2004, 67, 107-112.
35 Lugstein, A.; Jentys, A.; Vinek, H. Hydroisomerization and cracking of n-octane and C8 isomers on Ni-containing zeolites. Appl. Catal. A 1999, 176, 119−128.
36 Awala, H. ; Gilson, J.-P.; Retoux, R ; Boullay, P.; Goupil, J. -M.; Valtchev, V.; Mintova, S. Template-free nanosized faujasite-type zeolites. Nat. Mater. 2015, 14, 447−451.
37 Thibault-Starzyk, F.; Stan, I.; Abelló, S.; Bonilla, A.; Thomas, K.; Fernandez, C.; Gilson, J. P.; Pérez-Ramirez, J. Quantification of enhanced acid site accessibility in hierarchical
38 zeolites – The accessibility index. J. Catal. 2009, 264 (1), 11-14.
39 Qin, Z.; Cychosz, K. A.; Melinte, G.; El Siblani, H.; Gilson, J.-P.; Thommes, M.; Fernandez, C.; Mintova, S.; Ersen, O.; Valtchev, V. Opening the Cages of Faujasite-Type Zeolite. J. Am. Chem. Soc. 2017, 139, 17273−17276.
40 Kaduk, J. A.; Faber, J. Crystal structure of zeolite Y as a function of ion exchange. Rigaku Journal 1995, 12(2), 14-34
41 Tsuchida, T.; Furuichi, R.; Ishii, T. Kinetics of the dehydration of boehmites prepared under different hydrothermal conditions. Thermochimica Acta 1980, 39, 103-115.
42 Alphonse, P.; Courty, M. Structure and thermal behavior of nanocrystalline boehmite Thermochimica Acta 2005, 425, 75-89.
43 G. Busca, Chapter 3“Structural, Surface, and Catalytic Properties of Aluminas”, Adv. Catal, Jentoft, F. C. 2014, 57, 319-404.
44 Yu, Z.; Li, S.; Wang, Q.; Zheng, A.; Jun, X.; Chen, L. ; Deng, F. Brønsted/Lewis Acid Synergy in H–ZSM-5 and H–MOR Zeolites Studied by $^{1}H$ and $^{27}Al$ DQ-MAS Solid-State NMR Spectroscopy. J. Phys. Chem. C 2011, 115, 22320-22327.
45 Khabtou, S.; Chevreau, T.; Lavalley, J. C. Quantitative infrared study of the distinct acidic hydroxyl groups contained in modified Y zeolites. Microporous Mater. 1994, 3, 133-148.
46 Cairon, O.; Thomas, K.; Chevreau, T. FTIR studies of unusual OH groups in steamed HNaY zeolites: preparation and acid properties. Microporous Mesoporous Mater. 2001, 46, 327-340.
47 Crépeau, G.; Montouillout, V.; Vimont, A.; Mariey, L.; Cseri, T.; Mauge, F. Nature, Structure and Strength of the Acidic Sites of Amorphous Silica Alumina: An IR and NMR Study. J. Phys. Chem. B 2006, 110, 15172-15185.
48 Kondo, J. N.; Nishitani, R.; Yoda, E.; Yokoi, T.; Tatsumia, T.; Domenc, K. A comparative IR characterization of acidic sites on HY zeolite by pyridine and CO probes with silica–alumina and γ-alumina references Phys. Chem. Chem. Phys. 2010, 12, 11576–11586.
49 Mintova, S.; Gilson, J.-P.; Valtchev, V. Advances in nanosized zeolites, Nanoscale 2013, 5 (15), 6693-6703.
50 Degnan, T. F.; Smith, C. M.; Venkat, C. R. Alkylation of aromatics with ethylene and propylene: recent developments in commercial processes. Appl. Catal. A, 2001, 221, 283–294.
51 Corma, A.; Martínez-Soria, V.; Schnoeveld, E. Alkylation of Benzene with Short-Chain Olefins over MCM-22 Zeolite: Catalytic Behaviour and Kinetic Mechanism. J. Catal. 2000, 192, 163–173.
52 Vermeiren, W.; Gilson, J.-P. Impact of Zeolites on the Petroleum and Petrochemical Industry. Top. Catal. 2009, 52, 1131–1161